

Understanding the Stability for $LiNi_{0.5}Mn_{0.5}O_2$ as a Co-free positive electrode material

Xinyi Liu, Dongyan Zhang,* Zhimin Li,† Maolin Zhang, and Yangxi Yan
School of Advanced Materials and Nanotechnology, Xidian University, Xi'an 710126, China

PangPang Wang
Nanomaterials Group, Institute of System, Information Technologies and Nanotechnologies (ISIT),
Fukuoka Industry-Academia Symphoncity (FiaS),
4-1 Kyudaishinmachi, Nishi-ku, Fukuoka 819-0388, Japan

Ri-ichi Murakami
School of Mechanical Engineering, Chengdu University, Chengdu 610106, P. R. China
(Dated: February 10, 2022)

For understanding the stability of Co-free positive electrode material, $LiNi_{0.5}Mn_{0.5}O_2$ was synthesized with different addition amount of lithium during calcination. The valence states of transition metal in the prepared samples were determined by combining accurate stoichiometry analysis via ICP, magnetic moment measurement via SQUID, and element valence analysis via XPS with Ar ion etching. Unexpectedly, the transition metals, Ni and Mn, at interior and surface of $LiNi_{0.5}Mn_{0.5}O_2$ particles show different electrochemical properties. This answer lingering questions of Li de-intercalation mechanism in $LiNi_{0.5}Mn_{0.5}O_2$.

I. INTRODUCTION

Layered lithium nickel manganese oxides ($LiNi_xMn_{1-x}O_2$) are promising alternative positive electrode materials to the currently commercial $LiCoO_2$ and Ternary materials for lithium ion batteries (LIBs) [1, 2]. $LiNi_xMn_{1-x}O_2$ cathode materials are expected to possess as high theoretical capacity as $LiCoO_2$ of approximately $279 \text{ mAh} \cdot \text{g}^{-1}$ [3], which is based on assumptions that [4–7] (1). Nickel and manganese are Ni^{2+}, Mn^{4+} in $LiNi_xMn_{1-x}O_2$, (2). The Ni^{2+}/Ni^{4+} redox pairs contribute to electrochemical activity while all lithium ions are extracted, and Mn^{4+} ions remain as Mn^{4+} throughout the cycling process. However, several issues still doubt researchers including diverse reported specific capacities [8–12], capacity loss during the initial cycles [12–14], and poor lithium ion diffusivity [15, 16]. A lot of efforts have been made to elucidate these problems and to improve the electrochemical properties based on the above mentioned assumptions [8–16]. For example, the capacity loss during the initial cycles was considered to be arising from surface reaction of cathode with electrolyte, so various coating methods have been developed to isolate the cathode from electrolyte [16]; the poor rate capacity was considered to mainly be attributed to cation mixing at lithium site, so a strategy has been widely used that lattice was strained by ions doping to inhibit nickel occupying the lithium site [17]. This theory about Ni^{2+} and Mn^{4+} in $LiNi_xMn_{1-x}O_2$ originated from the conventional element valence analysis characterized by X-ray photoelectron spectroscopy (XPS) [18] and cyclic voltammetry [19]. However, XPS could only characterize

properties originating from surface several manometers [20], and redox potentials of Ni^{2+}/Ni^{3+} and Ni^{3+}/Ni^{4+} are close [19]. Hence, the deduction of Ni^{2+} and Mn^{4+} in $LiNi_xMn_{1-x}O_2$ is a fantasied edifice, and a lot of doubts hangs over thousands of researchers to bring the cobalt free layered lithium nickel manganese oxides into practical applications. The urgent task is to confirm the chemical structure of $LiNi_xMn_{1-x}O_2$.

Herein, valence states of transition metals in as-prepared cobalt free layered lithium nickel manganese oxides with nominal stoichiometry of $LiNi_{0.5}Mn_{0.5}O_2$ were determined by combining accurate stoichiometry analysis via ICP, magnetic moment measurement via SQUID, and depth-profiling valence via XPS. Unexpectedly, the transition metals, Ni and Mn, at interior and surface of $LiNi_{0.5}Mn_{0.5}O_2$ particles demonstrated different electrochemical properties. Ni at the surface of $LiNi_{0.5}Mn_{0.5}O_2$ was +2, but at interior was +3. Mn at the surface was +4, at interior was +3. XPS for the Mn 3s orbital with Ar ion etching $LiNi_{0.5}Mn_{0.5}O_2$ particles confirmed that binding energy presented significant difference for surface and interior. In the following, we should see such an inhomogeneous valence of transition metal indeed existed in as-prepared cobalt free layered lithium nickel manganese oxides, $LiNi_{0.5}Mn_{0.5}O_2$, and its influence on the stability and electrochemical properties.

II. EXPERIMENTAL

The cobalt free layered lithium nickel manganese oxide, $LiNi_{0.5}Mn_{0.5}O_2$, were prepared by sol-gel method using lithium acetate ($LiCH_3COO \cdot 2H_2O$, MACKLIN, 99.9%), nickel acetate ($Ni(CH_3COO)_2 \cdot 4H_2O$, Shanghai Chemical Reagent Research Institute, 98%), and manganese acetate ($Mn(CH_3COO)_2 \cdot 4H_2O$, Shanghai

* zhangdongyan@xidian.edu.cn

† zmli@mail.xidian.edu.cn

Chemical Reagent Research Institute, 90%) as source, citric acid as complexing agent. The samples were calcined at 900 °C for 16 h to obtain the final products after preparing the xerogel powders as procedures of dissolving metal salts in deionized water, adding citric acid, heating in water bath at 80°C for 4 hours to obtain sol, drying in vacuum drying oven at 120°C for 12 h to obtain xerogel, and grinding to powders. Due to the volatilization of lithium during calcination, 10%, 15%, and 20% excess $LiCH_3COO \cdot 2H_2O$ were added during the initial dissolution procedure, and the obtained products were denoted as L10, L15, and L20.

The crystal structure of prepared $LiNi_{0.5}Mn_{0.5}O_2$ samples was analyzed by X-ray diffractometry (XRD) using a Bruker D8 Advance apparatus equipped with a Cu K_α X-ray source ($\lambda = 1.5406 \text{ \AA}$). XRD measurements were collected in the 2θ range 10 – 80°. The stoichiometry of each sample was decided by inductively coupled plasma-optical emission spectrometry (ICP-OES) using Agilent 5100. Magnetic measurements for susceptibility were carried out with a fully automated magnetometer (MPMS-3 from Quantum Design) using a ultra-sensitive Superconducting Quantum Interface Device (SQUID) in the temperature range of 3-300 K. Chemical state identifications were made using XPS (Thermo Scientific K-Alpha⁺) with a monochromatic Al K_α source. The XPS data were collected before and after samples were etched by Ar ions with the depths of 20 nm and 40 nm. The electrochemical properties of the samples were tested at room temperature in cells with metallic lithium as anode electrode. Cell assembly and measurements were carried out following the experimental procedure previously described [21] using Land CT2991A laboratory-cell test system (Wuhan Jinnuo Electric Co. Ltd., China). Voltage curves were recorded at 0.05 C rate for initial charge-discharge cycle, and at 1C for the following capacity retention test.

III. RESULTS AND DISCUSSIONS

Figure 1 shows the XRD patterns of as-prepared Samples L10, L15, and L20. All patterns were indexed by a typical $\alpha - NaFeO_2$ hexagonal layered structure. The patterns for all samples did not display remarkable difference, indicating that the addition amount of excess lithium did not change the crystalline profile. However, some weak diffraction peaks between 20° and 25° were observed in XRD patterns of Samples L15, and L20. These are arising from the superlattice order of Li-Mn ions in transition-metal layers, demonstrating the existence of Li-rich Li_2MnO_3 phase. The existence of Li_2MnO_3 in Samples L15 and L20 was attributed to the massive overdose of $LiCH_3COO \cdot 2H_2O$ during synthesis process. The accurate stoichiometry of each sample was determined by ICP-OES.

Table I shows the stoichiometry and valence of cations in as-prepared samples decided by ICP-OES and SQUID.

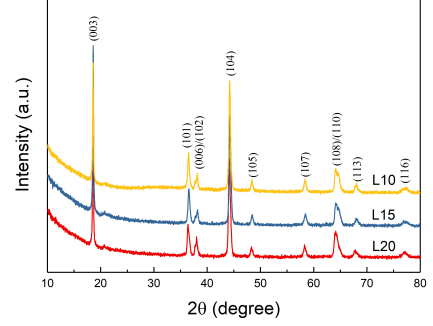


FIG. 1. XRD patterns of Samples L10, L15, and L20.

It demonstrates that the Ni/Mn mole ratio is close to the nominal value of 1:1, however due to the occupation of excess lithium at transition metal sites, the stoichiometry of Sample L15 and L20 deviate from the designed chemical formula, $LiNi_{0.5}Mn_{0.5}O_2$. Among the as-prepared samples, L10 approximately concurred with the design, but L15 and L20 possess excess lithium at transition metal site and the concentrations of Mn are little higher than that of Ni.

Because lithium possesses one 2s orbital electron, either lithium ions located at Li sites or transition metal sites should be valence of +1. Owing to the condition of electroneutrality, the average valence of cations located at transition metal sites should be +3. This indicates that nickel and manganese ions located at transition metal sites in $LiNi_{0.5}Mn_{0.5}O_2$ should be the pair of either Ni^{2+}/Mn^{4+} or Ni^{3+}/Mn^{3+} . Both nickel and manganese ions possess unpaired 3d orbital electrons resulting in magnetic moment, and nickel or manganese ions with different valence contributes different magnetic moments. Hence, the valence of nickel and manganese ions could be deduced from magnetic measurement data. Figure 2 shows the temperature dependence of the reciprocal magnetic susceptibility for Sample L10, L15, and L20. Above 200 K, the samples start to present a paramagnetic (PM) behavior which follows the Curie-Weiss law,

$$\chi = \frac{C_p}{T - \theta_p} \quad (1)$$

where C_p is the Curie constant and θ_p is the Weiss temperature. For temperature much higher than Curie temperature where samples behave like paramagnetic materials, the linear fit of the temperature dependence of the reciprocal magnetic susceptibility gives a Weiss constant θ_p and a Curie constant C_p . The fitted results are shown in Figure 2 and Table I. The negative θ_p value suggests that antiferromagnetic interactions are present in obtained $LiNi_{0.5}Mn_{0.5}O_2$. After the Curie constant, C_p , is determined experimentally by fitting the linear $\chi^{-1}(T)$ curve in the paramagnetic region, one can estimate the experimental value of effective moment μ_{eff} and then

TABLE I. The stoichiometry and valence for each element in each sample.

Sample	stoichiometry by ICP	θ_p	C_p	μ_{eff}	stoichiometry with Valence
L10	$Li(Li_{0.01}Ni_{0.49}Mn_{0.5})O_2$	-123 K	$2.30 \text{ emu} \cdot \text{K/mol}$	$4.32 \mu_B$	$Li(Li_{0.01}^{1+}Ni_{0.49}^{3+}Mn_{0.48}^{3+}Mn_{0.02}^{4+})O_2$
L15	$Li(Li_{0.1}Ni_{0.42}Mn_{0.48})O_2$	-109 K	$1.71 \text{ emu} \cdot \text{K/mol}$	$3.71 \mu_B$	$Li(Li_{0.1}^{1+}Ni_{0.03}^{2+}Ni_{0.39}^{3+}Mn_{0.25}^{3+}Mn_{0.23}^{4+})O_2$
L20	$Li(Li_{0.1}Ni_{0.44}Mn_{0.46})O_2$	-122 K	$1.72 \text{ emu} \cdot \text{K/mol}$	$3.72 \mu_B$	$Li(Li_{0.1}^{1+}Ni_{0.01}^{2+}Ni_{0.43}^{3+}Mn_{0.25}^{3+}Mn_{0.21}^{4+})O_2$

know the electronic configuration of the magnetic cation using the following equation[22],

$$\mu_{eff} = \sqrt{\frac{3k_B C_p}{N_A \mu_B^2}} = 2.84 \sqrt{C_p} \quad (2)$$

where N_A is the molar concentration of ions, μ_B the Bohr magneton, k_B the Boltzmann constant. The calculated effective moment μ_{eff} are listed in Table I. Combining the stoichiometry data by ICP-OES, the stoichiometry with valence for each element could be obtained according to the conservation of mass (Eqs. 3a and 3b), charge (Eq. 3c) and moment (Eq. 3d),

$$\sum n_{Ni^{i+}} = n_{Ni} \quad (3a)$$

$$\sum n_{Mn^{i+}} = n_{Mn} \quad (3b)$$

$$\sum i * n_{M^{i+}} = 3 \quad (3c)$$

$$\sum \mu_{M^{i+}} = \mu_{eff} \quad (3d)$$

where n is the concentration of each element, i represents the valence, M refers to the ions at transition metal site, μ indicates the magnetic moment. Sample L10 whose stoichiometry approximately concurred with the design possessed mainly Ni^{3+} and Mn^{3+} , while Samples L15 and L20 possess Ni^{2+} and Mn^{4+} besides of Ni^{3+} and Mn^{3+} .

Different from the widely reported that Mn in $LiNi_{0.5}Mn_{0.5}O_2$ is of Mn^{4+} to form the pair of Ni^{2+}/Mn^{4+} , the combination of ICP-OES and SQUID measurements demonstrate that the major of Mn in $LiNi_{0.5}Mn_{0.5}O_2$ is of Mn^{3+} . This difference is arising from the probing depth between SQUID and XPS. Magnetic measurement via SQUID collect the signal originating from the entire sample, but XPS probe the surface profile of the sample. Similar with reported in literature, the XPS data collected from the natural surface of sample L10 demonstrate Mn cations is mainly consist of Mn^{4+} according to the XPS of $Mn 3s$ orbital as shown in Figure 3. Combining with Ar ion etching, depth-profiling XPS analysis could be enabled. Herein, Ar ions were employed to etch the surface with 100 and 200 seconds into the depths of 20 nm and 40 nm. As the etching depth increases, the concentration of Mn^{3+} grows confirmed by the increasing in the energy difference between the multiplet states from 4.35 eV (Mn^{4+}) to 5.5 eV (Mn^{3+}) presented in Figure 3. Thus, we could conclude that the Mn^{4+} distributed at the surface of layered lithium nickel

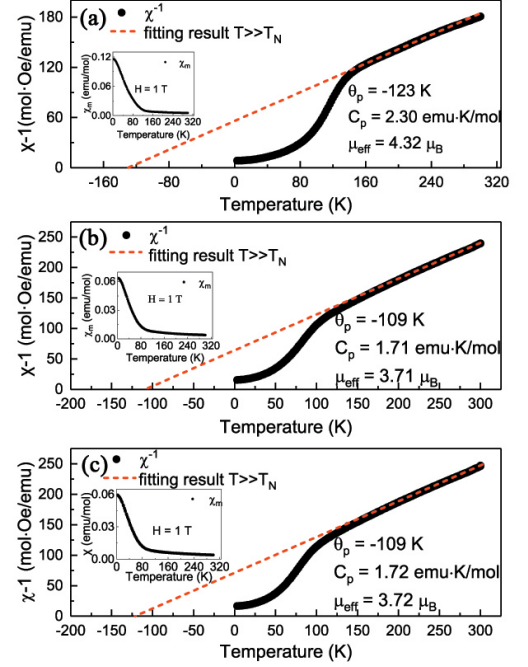
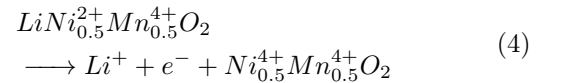


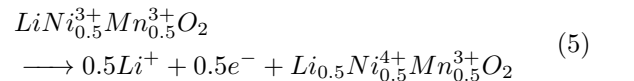
FIG. 2. Temperature dependence of the reciprocal magnetic susceptibility for (a) Sample L10, (b) Sample L15, (c) Sample L20. Insert shows the FC temperature dependence of the magnetic susceptibility.

manganese oxides to form $LiNi_{0.5}^{2+}Mn_{0.5}^{4+}O_2$ and Mn^{3+} centered the interior to form $LiNi_{0.5}^{3+}Mn_{0.5}^{3+}O_2$.

Because surface and interior of $LiNi_{0.5}Mn_{0.5}O_2$ behave different chemistry states, the delithiation rely on different redox thermodynamics. For surface



For interior



Due to the domination of Ni^{3+}/Mn^{3+} in $LiNi_{0.5}Mn_{0.5}O_2$, nearly half of the theoretical specific capacity could be delivered. During the lithiation, Ni^{4+}/Ni^{3+} redox occurred. Hence, existence of Ni^{2+} led to initial capacity loss. If Mn^{4+} concentration increased, the coulombic efficiency during initial charge/discharge

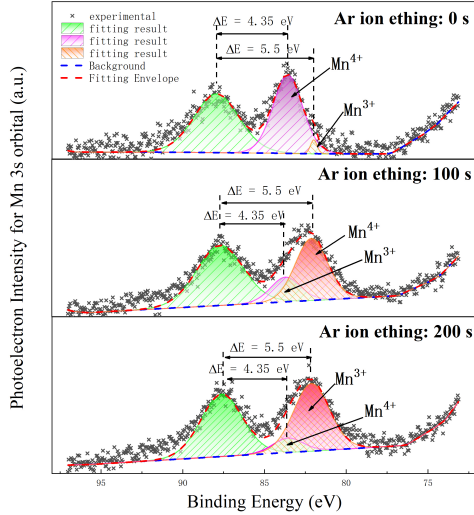


FIG. 3. XPS of $Mn\ 3s$ orbital for Sample L10 with different Ar ion etching depth.

cycle would be reduced. When the addition of lithium increase, excess Li^+ ions would occupied transition metal sites, resulting in double amount of manganese behave Mn^{4+} to balance the valence for an average of +3 at transition metal sites. The induced Mn^{4+} possesses more neighbour transition metal sites, resulting in some Ni^{2+} to achieve the local electric neutrality. As shown in Table I, and Ni^{2+} ions were identified in Sample L15 and L20. Due to the existence of Ni^{2+} and Li^+ at transition metal sites, the coulombic efficiency would be terrible during initial charge/discharge cycling. Figure 4 shows the charge/discharge profiles of assembled cells with L10, L15 and L20 cathode materials. As above discussed, assembled cells with Sample L10 cathode materials delivered average 130 mAh/g which is nearly half of the theoretical value of 279 mAh/g (assuming all lithium ions were extracted). When excess lithium were added, lithium-rich manganese oxides generated and excessive capacity was charged as shown in Figure 4a (L15 and L20). However, the excessive charged capacity was irreversible, and the discharged capacity reverted to the level of half theoretical value depending on the redox of Ni^{3+} (Figure 4).

IV. CONCLUSION

$LiNi_{0.5}Mn_{0.5}O_2$ with different addition amount of lithium was synthesized. The stoichiometry and valence states of transition-metal cations in as-prepared samples were analyzed by the combination of ICP-OES and SQUID measurements, which demonstrate the domination of Ni^{3+}/Mn^{3+} in as-prepared $LiNi_{0.5}Mn_{0.5}O_2$. XPS equipped with Ar ion etching was employed to analyze the distribution of Mn with different valence in

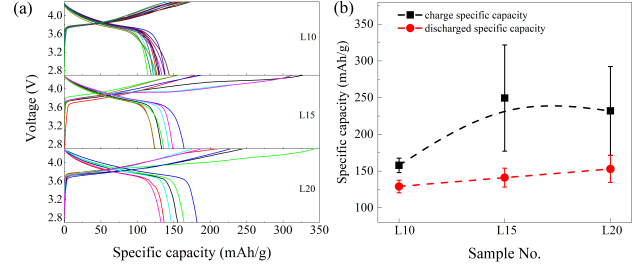


FIG. 4. (a) Charge/discharge specific capacity vs. voltage curves of assembled cells with L10, L15 and L20 cathode materials, (b) Statistical charge/discharge specific capacity for assembled cells with L10, L15, and L20 cathode materials.

the samples, which demonstrate that Mn^{4+} lay at surface and Mn^{3+} centered at the interior. This answer lingering questions of Li de-intercalation mechanism in $LiNi_{0.5}Mn_{0.5}O_2$ that half of the theoretical capacity was arising from the Ni^{3+}/Ni^{4+} redox, excess capacity from existence of lithium-rich manganese oxide, and capacity loss during the initial charge/discharge cycling owing to the existence of Ni^{2+} .

ACKNOWLEDGEMENT

This work was supported by the National Natural Science Foundation of China (Grant No. 52173227, 61974114), and the Fundamental Research Funds for the Central Universities (Grand No. JB211404).

- [1] G. Hu, Y. Shi, J. Fan, Y. Cao, Z. Peng, Y. Zhang, F. Zhu, Q. Sun, Z. Xue, Y. Liu, and K. Du, Sb doping and sb2o3 coating collaboration to improve the electrochemical performance of $lini_{0.5}mn_{0.5}o_2$ cathode material for lithium ion batteries, *Electrochimica Acta* **364**, 137127 (2020).
- [2] N. Voronina, Y.-K. Sun, and S.-T. Myung, Co-free layered cathode materials for high energy density lithium-ion batteries, *ACS Energy Letters* **5**, 1814 (2020).

- [3] X. Meng, S. Dou, and W. lou Wang, High power and high capacity cathode material $lini_{0.5}mn_{0.5}o_2$ for advanced lithium-ion batteries, *Journal of Power Sources* **184**, 489 (2008), selected papers from the: INTERNATIONAL BATTERY MATERIALS ASSOCIATION 2007 CONFERENCE. In Memoriam of Juergen Besenhard.
- [4] A. Celeste, M. Tuccillo, A. Santoni, P. Reale, S. Brutti, and L. Silvestri, Exploring a co-free, li-rich layered oxide with low content of nickel as a positive electrode for li-ion

- battery, *ACS Applied Energy Materials* **4**, 11290 (2021).
- [5] W.-S. Yoon, C. P. Grey, M. Balasubramanian, X.-Q. Yang, and J. McBreen, In situ x-ray absorption spectroscopic study on $\text{LiNi}_0.5\text{Mn}_0.5\text{O}_2$ cathode material during electrochemical cycling, *Chemistry of Materials* **15**, **16**, 3161–3169 (2003).
 - [6] A. Deb, U. Bergmann, S. P. Cramer, and E. J. Cairns, Local structure of $\text{LiNi}_0.5\text{Mn}_0.5\text{O}_2$ cathode material probed by in situ x-ray absorption spectroscopy, *Journal of Applied Physics* **99**, 063701 (2006), <https://doi.org/10.1063/1.2179198>.
 - [7] A. Abdel-Ghany, K. Zaghib, F. Gendron, A. Mauger, and C. Julien, Structural, magnetic and electrochemical properties of $\text{LiNi}_0.5\text{Mn}_0.5\text{O}_2$ as positive electrode for lithium batteries, *Electrochimica Acta* **52**, 4092 (2007).
 - [8] P. Manikandan, M. Ananth, T. Prem Kumar, M. Raju, P. Periasamy, and K. Manimaran, Solution combustion synthesis of layered $\text{LiNi}_0.5\text{Mn}_0.5\text{O}_2$ and its characterization as cathode material for lithium-ion cells, *Journal of Power Sources* **196**, 10148 (2011).
 - [9] B. Zhang, G. Chen, P. Xu, and C. C. Li, Effect of equivalent and non-equivalent Al substitutions on the structure and electrochemical properties of $\text{LiNi}_0.5\text{Mn}_0.5\text{O}_2$, *Journal of Power Sources* **176**, 325 (2008).
 - [10] D. Darbar, E. C. Self, L. Li, C. Wang, H. M. Meyer, C. Lee, J. R. Croy, M. Balasubramanian, N. Muralidharan, I. Bhattacharya, I. Belharouak, and J. Nanda, New synthesis strategies to improve Co-free $\text{LiNi}_0.5\text{Mn}_0.5\text{O}_2$ cathodes: Early transition metal d0 dopants and manganese pyrophosphate coating, *Journal of Power Sources* **479**, 228591 (2020).
 - [11] J. Yang, B. Guo, H. He, Y. Li, C. Song, and G. Liu, $\text{LiNi}_0.5\text{Mn}_0.5\text{O}_2$ hierarchical nanorods as high-capacity cathode materials for Li-ion batteries, *Journal of Alloys and Compounds* **698**, 714 (2017).
 - [12] C. Hu, J. Guo, J. Wen, Y. Peng, and Y. Chen, Preparation and electrochemical performance of $\text{LiNi}_0.5\text{Mn}_0.5\text{O}_2\text{-xFe}_x$ ($0 \leq x \leq 0.04$) cathode material synthesized with hydroxide co-precipitation for lithium ion batteries, *Journal of Alloys and Compounds* **581**, 121 (2013).
 - [13] H. Li, Q. Xu, X.-X. Shi, D.-W. Song, and L.-Q. Zhang, Electrochemical performance of $\text{LiNi}_0.5\text{Mn}_0.5\text{O}_2$ with different synthesis methods, *Rare Metals* **34**, 580–585 (2015).
 - [14] Y. Zhang, Y. Zhang, L. Wang, X. He, J. Yang, Y. Jin, and K. Zhang, Effect of cooling on the structure and electrochemical properties of $0.3\text{Li}_2\text{MnO}_3 \cdot 0.7\text{LiNi}_0.5\text{Mn}_0.5\text{O}_2$ cathode material, *Ionics* **21**, 1819–1825 (2015).
 - [15] N. Yabuuchi, Y.-C. Lu, A. N. Mansour, T. Kawaguchi, and Y. Shao-Horn, The influence of surface chemistry on the rate capability of $\text{LiNi}_{0.5}\text{Mn}_{0.5}\text{O}_2$ for lithium rechargeable batteries, *Electrochemical and Solid-State Letters* **13**, A158 (2010).
 - [16] A. Abdel-Ghany, R. El-Tawil, A. Hashem, A. Mauger, and C. Julien, Improved electrochemical performance of $\text{LiNi}_0.5\text{Mn}_0.5\text{O}_2$ by Li-enrichment and AlF₃ coating, *Materials* **5**, 100207 (2019).
 - [17] G. Jia, X. Shanguan, S. Liu, and Z. He, Improving the rate performance of $\text{LiNi}_0.5\text{Mn}_0.5\text{O}_2$ material at high voltages by Cu-doping, *Ionics* **26**, 4969–4976 (2020).
 - [18] R. A. Quinlan, Y.-C. Lu, Y. Shao-Horn, and A. N. Mansour, XPS studies of surface chemistry changes of $\text{LiNi}_0.5\text{Mn}_0.5\text{O}_2$ electrodes during high-voltage cycling, *Journal of The Electrochemical Society* **160**, A669 (2013).
 - [19] P. Periasamy and N. Kalaiselvi, Electrochemical performance behavior of combustion-synthesized $\text{LiNi}_0.5\text{Mn}_0.5\text{O}_2$ lithium-intercalation cathodes, *Journal of Power Sources* **159**, 1360 (2006).
 - [20] M. Aziz and A. Ismail, Chapter 5 - x-ray photoelectron spectroscopy (xps), in *Membrane Characterization*, edited by N. Hilal, A. F. Ismail, T. Matsuura, and D. Oatley-Radcliffe (Elsevier, 2017) pp. 81–93.
 - [21] J. Li, Z. Li, M. Zhang, Y. Yan, D. Zhang, P. Wang, and R.-i. Murakami, Correlated biphasic features of improved rate capability upon Ga doping in $\text{LiNi}_0.6\text{Mn}_0.2\text{Co}_0.2\text{O}_2$, *J. Mater. Chem. A* **9**, 23323 (2021).
 - [22] C. M. Julien, A. Ait-Salah, A. Mauger, and F. Gendron, Magnetic properties of lithium intercalation compounds, *Ionics* **12**, 21 (2006).